

Resonance-aware subtraction in the dipole method

Stefan Höche,^a Sebastian Liebschner,^b and Frank Siegert^b

^a*SLAC National Accelerator Laboratory, Menlo Park, CA, 94025, USA*

^b*Institut für Kern- und Teilchenphysik, TU Dresden, 01069 Dresden, Germany*

E-mail: shoeche@slac.stanford.edu, sebastian.liebschner@tu-dresden.de,
frank.siegert@cern.ch

ABSTRACT: We present a technique for infrared subtraction in next-to-leading order QCD calculations that preserves the virtuality of resonant propagators. The approach is based on the pseudo-dipole subtraction method proposed by Catani and Seymour in the context of identified particle production. As a first application, we compute $e^+e^- \rightarrow W^+W^-b\bar{b}$, which is dominated by top-quark pair production above the threshold. We compare the efficiency of our approach with a calculation performed using the standard dipole subtraction technique.

Contents

1	Introduction	1
2	Stating the problem	2
3	Pseudo-dipole subtraction	3
3.1	Catani-Seymour formalism	4
3.2	Application to resonance-aware subtraction	5
4	Application to $W^+W^-b\bar{b}$ Production in e^+e^- Collisions	9
4.1	Singular limits	9
4.2	Physical cross sections	10
5	Conclusions	12
A	Construction of phase-space trajectories	12

1 Introduction

The production and decay of heavy resonances like the top quark is of greatest interest in particle-physics phenomenology [1]. It presents a window into new physics, which is commonly believed to emerge in the form of new interactions at high energy. Precision measurements of Standard Model parameters at current collider energies may reveal parts of this structure if they can be made at high precision. However, the top quark cannot be considered an asymptotic state when performing the measurement, instead its existence as an intermediate state is inferred from its decay products. Radiative corrections to both production and decay are commonly simulated in computer programs called event generators, which allow to map experimental signatures associated with top-quark production to the parameters of the theory, in particular the pole mass or the $\overline{\text{MS}}$ mass of the top quark. It is the factorized approach of the simulation that presents a problem when the precision target of the measurement lies below the resonance width, because the narrow width approximation can no longer be applied [2]. A natural solution is to compute the complete final state at high precision using next-to-leading order calculations matched to parton showers [3, 4]. When doing so, attention must be paid to the fact that the process is an interplay of continuum contributions and resonant top-quark production, which could in principle be treated in the narrow-width approximation. On-shell top quark production mandates a special choice of kinematics mapping in the transition from Born to real-emission final states in the matching procedure. This problem has been addressed in great detail [5–9] in the context of the Frixione-Kunszt-Signer subtraction method [10], but no attempt has so far

been made to implement a solution based on Catani-Dittmaier-Seymour-Trocsanyi dipole subtraction [11, 12]. In this manuscript we therefore discuss the concept of a new technique that is based on the identified particle methods presented in [11] and apply the procedure to the computation of top-quark pair production at a future linear collider [13, 14] at NLO QCD accuracy. The method can straightforwardly be extended to hadron colliders, where measurements of singly- and doubly-resonant top-quark pair production have just been reported [15].

The outline of this paper is as follows: Section 2 introduces the problem of resonances in NLO calculations. Section 3 reviews the formalism of pseudo dipole subtraction as introduced in [11] and shows how it can be applied to resonance-aware subtraction. Section 4 presents a first application, and Sec. 5 gives an outlook.

2 Stating the problem

The calculation of observables at NLO requires the computation of real and virtual quantum corrections to the Born cross section. After renormalisation both these contributions are still separately infinite, although their sum is finite for infrared safe observables. In order to calculate such observables efficiently, general next-to-leading order infrared subtraction schemes have been devised, the most widely used being the methods by Frixione Kunszt and Signer (FKS) [10] and the ones by Catani and Seymour (CS) [11, 12]. Both methods are based on the extraction of the singular limits of the real-emission corrections, their analytic integration and combination of the result with the virtual corrections to render both real-emission and virtual corrections separately infrared finite. Focusing, for simplicity, on the total cross section in a process with no initial state hadrons, we can write schematically

$$\sigma^{\text{NLO}} = \int_m (\text{d}\sigma^{\text{B}} + \text{d}\sigma^{\text{V}} + \text{d}\sigma^{\text{I}}) + \int_{m+1} (\text{d}\sigma^{\text{R}} - \text{d}\sigma^{\text{S}}). \quad (2.1)$$

Here $\int_m \text{d}\sigma^{\text{I}} = \int_{m+1} \text{d}\sigma^{\text{S}}$ is the subtraction term, which is analytically integrated over the phase-space of the additional parton in the real correction and \int_m indicates that the phase-space integral corresponds to m final-state partons.¹ In the remainder of this paper we will focus on CS dipole subtraction [11]. In processes with intermediate resonances, this technique exhibits an undesired feature, which can most easily be explained using a concrete example, say $e^+e^- \rightarrow W^+W^-b\bar{b}$. If the center-of-mass energy is greater than the top pair threshold $\sqrt{s} \gtrsim 2m_t$, this process is dominated by on-shell $t\bar{t}$ -production and decay.

One possible real emission correction to this process is depicted on the left-hand side of Fig. 1. The subtraction term associated to the collinear singularity is constructed from the Born-diagram on the right-hand side of Fig. 1, and its kinematics is obtained by mapping the on-shell final-state momenta of the real correction to the Born using the algorithm in [11]. In the canonical method, the momenta of the emitter (\bar{b} -quark) and the spectator (b -quark) are adjusted, while all other momenta remain the same. This procedure generates a recoil that is indicated by the dashed line in Fig. 1. The recoil leads to the subtraction

¹Our analysis focuses on NLO QCD corrections, though the method can be extended to include NLO electroweak corrections.

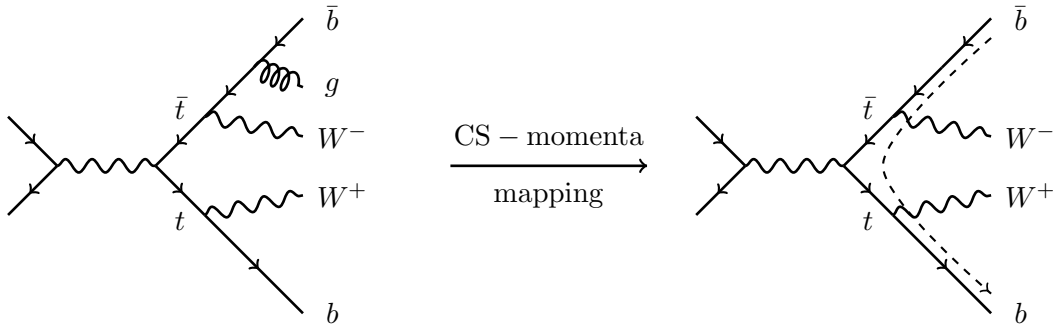


Figure 1. Possible real correction configuration for $W^+W^-b\bar{b}$ production and Born configuration of associated standard CS-dipole. The curved arrow on the right indicates the flow of the recoil.

term being evaluated at different virtualities of the intermediate top-quarks than the real-emission diagrams whose divergences it counteracts. As the top-quark propagator scales like $(p_t^2 - m_t^2 + im_t\Gamma_t)^{-1}$ and $\Gamma_t \ll m_t$, the change in virtuality may cause numerically large deviations between the real-emission corrections and the corresponding subtraction terms. Though the cancellation of infra-red divergences still takes place, the associated large weight fluctuations may significantly affect the convergence of the Monte-Carlo integration. The problem becomes manifest when interfacing the fixed-order NLO calculation to a parton shower. The difference in matrix-element weights arising from resonant propagators being shifted off resonance by means of adding radiation and mapping momenta from Born to real-emission kinematics bears no relation with the logarithms to be resummed by the parton shower, yet its numerical impact may be similar. This motivates the usage of an improved kinematics mapping by means of pseudo-dipoles.

3 Pseudo-dipole subtraction

The concept of pseudo-dipoles was introduced in [11] to cope with the situation where a subset of the final-state partons lead to the production of identified hadrons. In such a scenario, both emitter and spectator of a dipole may be “identified” in the sense that they fragment into identified hadrons. Because the directions of the identified hadrons are measurable, neither emitter nor spectator parton in the dipole can be allowed to absorb the recoil when mapping the momenta of the real-emission final state to a Born configuration. Instead the kinematics is balanced by adjusting the momenta of all non-identified final state particles (not just partons). This idea is reminiscent of standard dipoles with initial-state emitter and initial-state spectator. In fact pseudo-dipoles may be thought of as a generalization of these configurations.

In the following, we will review the definition of the pseudo-dipole, describing a $q \rightarrow qg$ splitting, as they have been introduced in [11] and proceed to explain how they can be exploited for the purpose of resonance-aware subtraction.

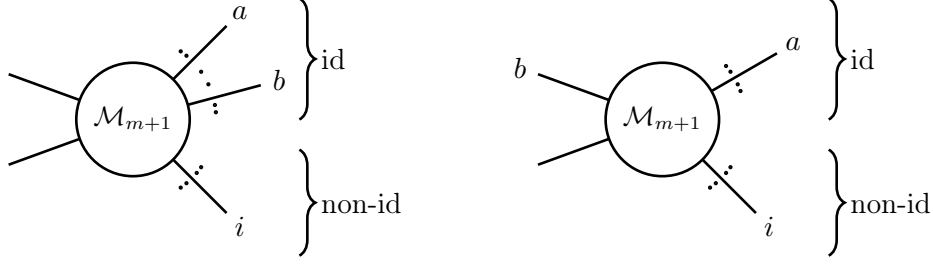


Figure 2. Labeling for pseudo-dipoles with final-state singularity. Left: Identified final-state spectator. Right: Initial-state spectator.

3.1 Catani-Seymour formalism

In order to satisfy the constraint that both emitter and spectator retain their direction, an additional momentum must be introduced that can absorb the recoil in the momentum mapping from real-emission to Born kinematics. This auxiliary momentum is defined as

$$n^\mu = p_{\text{in}}^\mu - \sum_{\alpha \in \{\text{id}\}} p_\alpha^\mu, \quad (3.1)$$

where p_{in} is the total incoming momentum in the process, and the sum runs over all outgoing identified particles. The eventual dependence of the subtraction term on n^μ accounts for the term *pseudo-dipole*. An immediate consequence of this definition is that there are only two types of pseudo-dipoles, because the spectator momentum is always in the final state. This is in contrast to standard Catani-Seymour dipoles, which have four different types, corresponding to all combinations of initial-state or final-state emitter with initial-state or final-state spectator. We denote pseudo-dipoles with final-state emitter as $\mathcal{D}_{ai,b}^{(n)}$ and pseudo-dipoles with initial-state emitter as $\mathcal{D}_b^{(n)ai}$.

The pseudo-dipole for splittings of final state partons reads [11]

$$\mathcal{D}_{ai,b}^{(n)} = -\frac{1}{2p_a p_i} \left\langle \dots, \tilde{a}i, \dots, b, \dots \left| \frac{\mathbf{T}_b \mathbf{T}_{ai}}{\mathbf{T}_{ai}^2} \mathbf{V}_{ai,b}^{(n)} \right| \dots, \tilde{a}i, \dots, b, \dots \right\rangle_{m,a,\dots}, \quad (3.2)$$

where a refers to an identified final state parton (the emitter) and the color spectator b may either be another identified final state parton or an initial state parton. This situation is depicted in Fig. 2. The kinematics in the correlated Born matrix element is given as follows: The momentum of the emitter is scaled as

$$\tilde{p}_{ai}^\mu = \frac{1}{z_{ain}} p_a^\mu \quad \text{where} \quad z_{ain} = \frac{p_a n}{(p_a + p_i)n}. \quad (3.3)$$

All non-identified particles (not just partons) in the final state are Lorentz-transformed by

$$\tilde{k}_j^\mu = \Lambda_\nu^\mu(K, \tilde{K}) k_j^\nu \quad \text{where} \quad (3.4)$$

$$\Lambda_\nu^\mu(K, \tilde{K}) = g_\nu^\mu - \frac{2(K + \tilde{K})^\mu (K + \tilde{K})_\nu}{(K + \tilde{K})^2} + \frac{2\tilde{K}^\mu K_\nu}{K^2}. \quad (3.5)$$

The momenta K^μ and \tilde{K}^μ are given by

$$K^\mu = n^\mu - p_i^\mu \quad (3.6)$$

$$\tilde{K}^\mu = n^\mu - (1 - x_{ain})p_a^\mu \quad \text{where} \quad x_{ain} = \frac{(p_a - p_i)n}{p_a n}. \quad (3.7)$$

The remaining momenta, namely those of identified and initial state particles (in particular of parton b) remain unchanged.

The complete list of pseudo-dipole insertion operators is given in [11]. As we focus on processes with no final-state gluons at Born level, the only one relevant to our computations is the $q \rightarrow qg$ insertion operator, which reads

$$\langle s \left| \mathbf{V}_{q_a g_i, b}^{(n)} \right| s' \rangle = 8\pi\mu^{2\epsilon} \alpha_s C_F \left[2 \frac{v_{i,ab}}{z_{ain}} - (1 + z_{ain}) - \epsilon(1 - z_{ain}) \right] \delta_{ss'}, \quad (3.8)$$

where

$$v_{i,ab} = \frac{p_a p_b}{p_i(p_a + p_b)}. \quad (3.9)$$

The integrated splitting kernel is defined as

$$\frac{\alpha_s}{2\pi} \frac{1}{\Gamma(1 - \epsilon)} \left(\frac{4\pi\mu^2}{2p_a p_b} \right)^\epsilon \bar{\mathcal{V}}_{ai,a} := \int [dp_i(n, p_a, z)] \frac{1}{2p_a p_i} \langle \mathbf{V}_{ai,b}^{(n)}(z_{ain}; v_{iab}) \rangle. \quad (3.10)$$

where $[dp_i(n, p_a, z)]$ is the one-emission phase-space integral obtained by factorizing the real-emission phase space. One obtains

$$\begin{aligned} \bar{\mathcal{V}}_{q,q}(z; \epsilon; p_a, p_b, n) = & -\frac{1}{\epsilon} P^{qq}(z) + \delta(1 - z) V_{qq}(\epsilon) + \tilde{K}^{qq}(z) + \bar{K}^{qq}(z) + P^{qq}(z) \ln z \\ & + \mathcal{L}^{q,q}(z; p_a, p_b, n) + \mathcal{O}(\epsilon), \end{aligned} \quad (3.11)$$

where $V_{qq}(\epsilon)$ comprises all singularities needed to cancel the poles present in the virtual corrections. It is given in Eq. (5.32) of [11], and all other functions are listed in Appendix C of [11]. The single poles proportional to the Altarelli-Parisi splitting functions do not appear in the standard CS integrated dipole terms. They are canceled by collinear mass factorization counterterms, which – in our approach – can be viewed as the one-loop contribution to the partonic fragmentation function to be convoluted with the subtracted hard cross section. Before proceeding to the definition of the integrated dipole terms in form of **H**- and **P**-operators we will first explain how to apply pseudo-dipoles to resonant processes.

3.2 Application to resonance-aware subtraction

Pseudo-dipole subtraction terms that preserve the invariant mass of intermediate resonances can be constructed using the following algorithm:

1. If the emitter is the decay product of a resonance and the spectator is not a decay product of the same resonance, the dipole is replaced by a pseudo-dipole where the emitter and all particles except for the emission and the remaining decay products of the resonance are identified. This rule takes precedence.

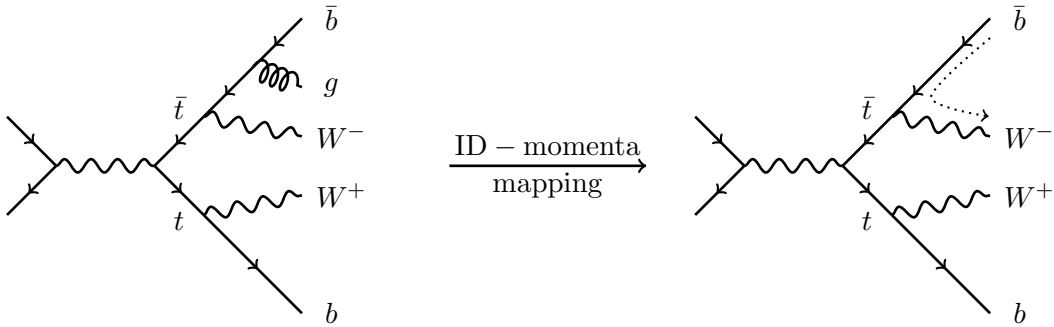


Figure 3. Possible real correction configuration for $W^+W^-b\bar{b}$ production and Born configuration of associated pseudo-dipoles. The curved arrow on the right indicates the flow of the recoil.

2. If the spectator is the decay product of a resonance and the emitter is not a decay product of the same resonance, the dipole is replaced by a pseudo-dipole where the emitter and all decay products of the resonance to which the spectator belongs are identified.
3. If emitter and spectator are decay products of the same resonance, the standard CS subtraction formalism is used.

It is clear that these rules can only be applied unambiguously once the diagrammatic structure of the real-emission corrections is simple enough for a clear assignment of “decay products” to be made. Despite this severe restriction, the algorithm can be used in a variety of processes, among them the highly relevant example of top-quark pair production, both at hadron and at lepton colliders.

Consider again the example $e^+e^- \rightarrow W^+W^-b\bar{b}$. If $\sqrt{s} > 2m_t$ the dominant contribution to the cross section stems from diagrams like the one on the left-hand side of Fig. 1. The standard CS dipole to cover the collinear singularity associated to this diagram is constructed by using the Born-level diagram on the right-hand side of Fig. 1. In this situation the recoil from the emitter parton \bar{b} to the spectator parton b affects the potentially resonant top quark propagators. To avoid this, we replace by means of the above algorithm the standard CS dipole by a pseudo-dipole and formally “identify” particles. As the first rule takes precedence we identify \bar{b} , W^+ and b . In this manner, the W^- boson is the only particle left to absorb the recoil. Hence the momentum of the top-quarks are unaltered and we have achieved our aim. The momentum flow corresponding to this situation is depicted in Fig. 3. The same reasoning is applied to the pseudo-dipole in which the b quark is the emitter.

We stress at this point that we do not actually identify particles throughout the calculation. Instead we integrate over all final-state momenta by means of adding partonic fragmentation functions. We will show in the following how this affects the **H**- and **P**-terms given in [11]. For simplicity, we consider a configuration with no initial state partons and m final state (anti-)quarks at Born level. In the following, the integration over non-QCD particles shall be understood whenever we write $\int_m d\phi_m$.

For now we will not integrate over the momentum of the merged parton \tilde{ai} . We denote this with a subscript -1 at the integral sign. The integral over the pseudo-dipoles is then given by

$$\begin{aligned}
\int_{m+1-1} d\sigma^S &= \mathcal{N}_{in} \sum_{\{m+1\}} \int_{m+1-1} d\phi_{m+1-1} \frac{1}{S_{\{m+1\}}} \sum_{\substack{\text{pairs } b \neq a, i \\ a, i}} \sum \mathcal{D}_{ai, b}^{(n)} F_J^{(m)} \\
&= -\mathcal{N}_{in} \int_0^1 \frac{dz}{z^{2-2\epsilon}} \sum_{\tilde{ai}=1}^m \sum_{\{m\}} \int_{m-1} d\phi_{m-1} \frac{1}{S_{\{m\}}} F_J^{(m)} \sum_{\substack{b=1 \\ b \neq \tilde{ai}}}^m |\mathcal{M}_m^{\tilde{ai} b}|^2 \\
&\quad \times \frac{\alpha_s}{2\pi} \frac{1}{\Gamma(1-\epsilon)} \left(\frac{4\pi\mu^2}{2p_a p_b} \right)^\epsilon \frac{1}{\mathbf{T}_{\tilde{ai}}^2} \bar{\mathcal{V}}_{\tilde{ai}, a}(z; \epsilon; p_a, p_b, n) \delta_{\tilde{ai} a}. \quad (3.12)
\end{aligned}$$

Here z is used as a shorthand notation for z_{ain} , given in Eq. (3.3). As we are concerned with $q \rightarrow qg$ splittings only, \tilde{ai} and a are always quarks. The corresponding integrated splitting function is given in Eq. (3.11). Each identified final-state parton contributes a collinear mass factorization counterterm

$$\begin{aligned}
\int_{m-1} d\sigma_a^C(p_a) &= -\frac{\alpha_s}{2\pi} \frac{1}{\Gamma(1-\epsilon)} \int_0^1 \frac{dz}{z^{2-2\epsilon}} \delta_{\tilde{ai} a} \\
&\quad \times \left[-\frac{1}{\epsilon} \left(\frac{4\pi\mu^2}{\mu_F^2} \right)^\epsilon P_{\tilde{ai} a}(z) + H_{\tilde{ai} a}^{F.S.}(z) \right] \int_{m-1} d\sigma_{\tilde{ai}}^B \left(\frac{p_a}{z} \right). \quad (3.13)
\end{aligned}$$

where the Born cross-section is given by

$$\int_m d\sigma^B = \mathcal{N}_{in} \sum_{\{m\}} \int_m d\phi_m \frac{1}{S_{\{m\}}} F_J^{(m)} |\mathcal{M}_m|^2. \quad (3.14)$$

When we add Eq. (3.12) and sum Eq. (3.13) for all identified partons, we can define an insertion operator:

$$\sum_{\tilde{ai}=1}^m \sigma^I(p_a) := \int_{m+1-1} d\sigma^S + \sum_{a=1}^m \int_{m-1} d\sigma_a^C =: \sum_{\tilde{ai}=1}^m \int_0^1 \frac{dz}{z^{2-2\epsilon}} \int_{m-1} d\sigma^B \left(\frac{p_a}{z} \right) \cdot \hat{\mathbf{I}}_{\tilde{ai}} \quad (3.15)$$

where $d\sigma^B \left(\frac{p_a}{z} \right) \cdot \hat{\mathbf{I}}_{\tilde{ai}}$ indicates that the squared Born matrix element in Eq. (3.14) is replaced by the spin- and color-correlated Born matrix element. Note that the parton \tilde{ai} in this expression carries momentum $\tilde{p}_{ai} = p_a/z$. The insertion operator is given by

$$\begin{aligned}
\hat{\mathbf{I}}_{\tilde{ai}} &= -\frac{\alpha_s}{2\pi} \frac{1}{\Gamma(1-\epsilon)} \left\{ \sum_{\substack{b=1 \\ b \neq \tilde{ai}}}^m \frac{\mathbf{T}_{\tilde{ai}} \mathbf{T}_b}{\mathbf{T}_{\tilde{ai}}^2} \left(\frac{4\pi\mu^2}{2p_a p_b} \right)^\epsilon \delta_{\tilde{ai} a} \bar{\mathcal{V}}_{q, q}(z; \epsilon; p_a, p_b, n) \right. \\
&\quad \left. + \delta_{\tilde{ai} a} \left[-\frac{1}{\epsilon} \left(\frac{4\pi\mu^2}{\mu_F^2} \right)^\epsilon P_{\tilde{ai} a}(z) + H_{\tilde{ai} a}^{F.S.}(z) \right] \right\}. \quad (3.16)
\end{aligned}$$

From this expression we extract the insertion operator $\mathbf{I}_{\tilde{ai}}$, which comprises all singularities and is identical to the one for standard FF-dipoles:

$$\mathbf{I}_{\tilde{ai}}(p_1, \dots, p_a, \dots, p_m; \epsilon) = -\frac{\alpha_s}{2\pi} \frac{1}{\Gamma(1-\epsilon)} \sum_{\substack{b=1 \\ b \neq \tilde{ai}}}^m \frac{\mathbf{T}_{\tilde{ai}} \mathbf{T}_b}{\mathbf{T}_{\tilde{ai}}^2} \left(\frac{4\pi\mu^2}{2p_a p_b} \right)^\epsilon \mathcal{V}_{qg}(\epsilon). \quad (3.17)$$

We split the remainder into **H**- and **P**-operators as

$$\hat{\mathbf{I}}_{\tilde{a}i} = \delta(1-z)\mathbf{I}_{\tilde{a}i} + \mathbf{H}_{\tilde{a}i} + \mathbf{P}_{\tilde{a}i}. \quad (3.18)$$

In order to combine the μ_F -dependent terms with the collinear counterterms, we used the identity $\sum_{\substack{b=1 \\ b \neq \tilde{a}i}}^m \mathbf{T}_b = -\mathbf{T}_{\tilde{a}i}$, which arises from color conservation [11]. After a few steps, we find up to $\mathcal{O}(\epsilon)$:

$$\mathbf{P}_{\tilde{a}i} \left(p_1, \dots, \frac{p_a}{z}, \dots, p_m; z; \mu_F \right) = \frac{\alpha_s}{2\pi} \sum_{\substack{b=1 \\ b \neq \tilde{a}i}}^m \frac{\mathbf{T}_{\tilde{a}i} \mathbf{T}_b}{\mathbf{T}_{\tilde{a}i}^2} \ln \frac{z\mu_F^2}{2p_a p_b} \delta_{\tilde{a}i} \mathbf{P}_{\tilde{a}i} \mathbf{P}_{\tilde{a}i} (z) \quad (3.19)$$

and

$$\begin{aligned} \mathbf{H}_{\tilde{a}i} (p_1, \dots, p_a, \dots, p_m; n; z) = & \\ & - \frac{\alpha_s}{2\pi} \left\{ \sum_{\substack{b=1 \\ b \neq \tilde{a}i}}^m \frac{\mathbf{T}_{\tilde{a}i} \mathbf{T}_b}{\mathbf{T}_{\tilde{a}i}^2} \delta_{\tilde{a}i} \mathbf{a} \left[\overline{K}^{\tilde{a}i} \mathbf{a} (z) + 2P_{\tilde{a}i} \mathbf{a} (z) \ln z + \tilde{K}^{\tilde{a}i} \mathbf{a} (z) \right. \right. \\ & \left. \left. + \mathcal{L}^{\tilde{a}i} \mathbf{a} (z; p_a, p_b, n) \right] + \delta_{\tilde{a}i} \mathbf{a} H_{\tilde{a}i}^{F.S.} (z) \right\}. \end{aligned} \quad (3.20)$$

In contrast to the original pseudo-dipole approach, we now replace the integration over p_a by an integration over the Born momentum $\tilde{p}_{ai} = p_a/z$ (see e.g. Ref. [16], p.24). This leads to the following transformation:

$$\int \frac{d^{D-1} p_a}{2|\vec{p}_a|} = z^{2-2\epsilon} \int \frac{d^{D-1} \tilde{p}_a}{2|\vec{\tilde{p}}_a|}. \quad (3.21)$$

The Jacobian of the transformation exactly cancels the prefactor $1/z^{2-2\epsilon}$ in Eq. (3.15). We thus obtain

$$\sum_{\tilde{a}i=1}^m \int \frac{d^D p_a}{(2\pi)^{D-1}} \delta(p_a^2) \sigma^I(p_a) = \sum_{\tilde{a}i=1}^m \int_m d\sigma^B(p_1, \dots, p_m) \int_0^1 dz \left[\delta(1-z)\mathbf{I}_{\tilde{a}i} + \mathbf{H}_{\tilde{a}i} + \mathbf{P}_{\tilde{a}i} \right]. \quad (3.22)$$

The momentum of parton $\tilde{a}i$ is \tilde{p}_{ai} and thus no longer z -dependent. This allows to simplify the operators. Setting $H_{qq}^{F.S.}(z) = 0$ (which corresponds to the $\overline{\text{MS}}$ -scheme), we obtain

$$\int_0^1 dz \delta(1-z)\mathbf{I}_{\tilde{a}i} (p_1, \dots, p_m; \epsilon) = -\frac{\alpha_s}{2\pi} \frac{1}{\Gamma(1-\epsilon)} \sum_{\substack{b=1 \\ b \neq \tilde{a}i}}^m \frac{\mathbf{T}_{\tilde{a}i} \mathbf{T}_b}{\mathbf{T}_{\tilde{a}i}^2} \left(\frac{4\pi\mu^2}{2\tilde{p}_{ai} p_b} \right)^\epsilon \mathcal{V}_{qq}(\epsilon) \quad (3.23)$$

$$\int_0^1 dz \mathbf{P}_{\tilde{a}i} (p_1, \dots, p_m; z; \mu_F) = \int_0^1 dz \frac{\alpha_s}{2\pi} \sum_{\substack{b=1 \\ b \neq \tilde{a}i}}^m \frac{\mathbf{T}_{\tilde{a}i} \mathbf{T}_b}{\mathbf{T}_{\tilde{a}i}^2} \ln \frac{\mu_F^2}{2\tilde{p}_{ai} p_b} P_{qq}(z) = 0. \quad (3.24)$$

Note that $\mathbf{P}_{\tilde{a}i}$ vanishes because $P_{qq}(z)$ is a pure plus distribution. We finally obtain

$$\begin{aligned}
& \int_0^1 dz \mathbf{H}_{\tilde{a}i}(p_1, \dots, p_a, \dots, p_m; n; z) \\
&= -\frac{\alpha_s}{2\pi} \sum_{\substack{b=1 \\ b \neq \tilde{a}i}}^m \frac{\mathbf{T}_{\tilde{a}i} \mathbf{T}_b}{\mathbf{T}_{\tilde{a}i}^2} \int_0^1 dz \left(\overline{K}^{qq}(z) + 2P_{qq}(z) \ln z + \tilde{K}^{qq}(z) + \mathcal{L}^{qq}(z; p_a, p_b, n) \right) \\
&= -\frac{\alpha_s}{2\pi} \sum_{\substack{b=1 \\ b \neq \tilde{a}i}}^m \mathbf{T}_{\tilde{a}i} \mathbf{T}_b \left\{ \frac{1}{4} + 2 \left[\text{Li}_2 \left(1 - \frac{1+v}{2} \frac{(\tilde{p}_{ai} + p_b)n}{\tilde{p}_{ai}n} \right) + \text{Li}_2 \left(1 - \frac{1-v}{2} \frac{(\tilde{p}_{ai} + p_b)n}{\tilde{p}_{ai}n} \right) \right] \right. \\
&\quad \left. + \int_0^1 dz (1+z) \ln \frac{n_z^2 \tilde{p}_{ai} p_b}{2z(\tilde{p}_{ai} n_z)^2} \right\}. \tag{3.25}
\end{aligned}$$

The last line of Eq. (3.25) is the only z -dependent contribution which cannot be integrated analytically. Note in particular that n_z implicitly depends on z through Eq. (3.1), where the momentum of the emitter particle is given by $p_a = z\tilde{p}_{ai}$.

We remark that the introduction of the collinear counterterms in Eq. (3.13) is actually unnecessary, since they give a vanishing contribution to the cross-section. This is due to $P_{qq}(z)$ being a pure plus-distribution and the test-function with which it is convoluted not being z -dependent after we substituted $p_a = z\tilde{p}_{ai}$. This is also true for differential cross-sections, since any partonic observable can be expressed without reference to z . The vanishing effect of collinear counterterms may also be understood from another point of view: As we do not actually restrict the momenta of the ‘‘identified’’ partons, but integrate over them eventually, we have already collected all singularities necessary to cancel those present in the virtual corrections. Hence, no collinear mass factorization counterterms are required.

4 Application to $W^+W^-b\bar{b}$ Production in e^+e^- Collisions

We have tested the above described resonance-aware subtraction by means of pseudo-dipoles in the reaction $e^+e^- \rightarrow W^+W^-b\bar{b}$. In the following we are going to compare results obtained with standard CS dipoles to those obtained with pseudo-dipoles for fixed NLO QCD predictions. In Sec. 4.1, we first examine the cancellation of divergences between the real-emission matrix elements and the different dipoles using ensembles of dedicated trajectories in phase-space, which approach the collinear and soft limits in a controlled way. Following this, we compare physical cross-sections calculated with the different subtraction techniques while paying special attention to the rate of convergence in the Monte-Carlo integration.

4.1 Singular limits

The only real-emission correction to the process $e^+e^- \rightarrow W^+W^-b\bar{b}$ at NLO is the process with an additional gluon in the final state. We are therefore confronted with two different

singular limits, namely the one with a soft gluon and the one with a collinear (anti-)quark-gluon pair. We use the following variables to parametrize the soft and collinear limits

$$y_{gb} = \frac{2p_g p_b}{(p_g + p_b + p_b)^2} \quad \text{and} \quad y_{g\bar{b}} = \frac{2p_g p_{\bar{b}}}{(p_g + p_b + p_b)^2}. \quad (4.1)$$

In the collinear limits, $y_{gb} \rightarrow 0$ or $y_{g\bar{b}} \rightarrow 0$, while in the soft limit $y_{gb}y_{g\bar{b}} \rightarrow 0$. To study the behavior of the subtraction when approaching these limits, we construct ensembles of trajectories in two steps: random phase-space points are sampled according to the real-emission cross section in the narrow-width approximation while requesting three identified jets in the Durham algorithm [17]. Subsequently, for each phase-space point the kinematical configuration is scaled according to the algorithm described in App. A to approach the soft or collinear limit.

The two plots in Fig. 4 display the values of the real-emission matrix-element, $R = |\mathcal{M}_R|^2$ and the two different sums of the associated dipoles ($S = \sum \mathcal{D}$), as well as the absolute value of their difference and their ratio for the soft (upper panel) and $b\bar{g}$ -collinear (lower panel) limit. Note that also the real-emission contribution is different between the two cases because for a fair comparison the construction of the soft/collinear limits is tailored to the kinematics mapping of the CS and ID cases respectively.

It can be seen that the cancellation of divergences works well in the standard CS subtraction method and in the pseudo-dipole approach, but that the pseudo-dipoles converge faster towards the real-emission matrix element. One would therefore also expect the Monte-Carlo integration to converge faster when pseudo-dipoles are used for subtraction.

4.2 Physical cross sections

In this section we present first results validating the pseudo-dipole subtraction method for resonance aware processes at the level of cross sections and distributions. Again we investigate the reaction $e^+e^- \rightarrow W^+W^-b\bar{b}$. Results are cross-checked using two different implementations of our new algorithm within the public event generation framework Sherpa [18, 19], one using the matrix-element generator AMEGIC++ [16, 20], and one in the new OpenLoops interface of Sherpa [21]. In the latter interface, the correlated Born matrix-elements are imported from OpenLoops libraries, while the splitting function is calculated in Sherpa and the integration is performed using the techniques implemented in AMEGIC++ [20]. We vary the center-of-mass energy of the collider to obtain predictions below, at and above the top-quark pair production threshold, and we do not include the effects of initial-state radiation. We require two hard jets at $y = (5 \text{ GeV}/E_{\text{cms}})^2$ defined according to the Durham algorithm [17]. The running of the strong coupling is evaluated at two loops, and the reference value is $\alpha_s(M_Z^2) = 0.118$, where $M_Z = 91.1876 \text{ GeV}$.

Table 1 shows the total cross sections as well as the individual contributions from the subtracted real-emission terms (RS) as well as Born, virtual corrections and integrated subtraction terms (BVI). As expected, the RS and BVI contributions differ between the standard CS subtraction method and the pseudo-dipole approach, but their sum agrees within the statistical accuracy of the Monte-Carlo integration. It can be seen that above and at the production threshold for a top-quark pair, the cross section for $e^+e^- \rightarrow W^+W^-b\bar{b}$ is

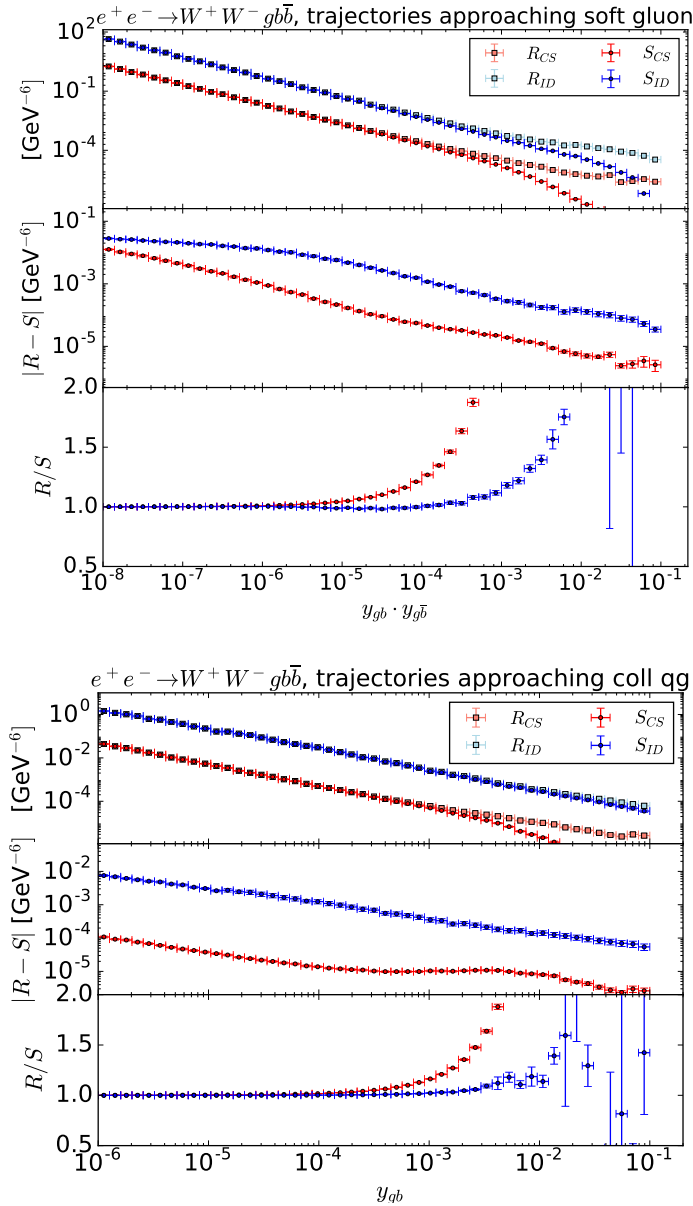


Figure 4. Matrix elements $R = |\mathcal{M}_R|^2$ and sum of associated dipoles $S = \sum \mathcal{D}$ (standard CS-dipoles in red, pseudo-dipoles in blue) for the process $e^+e^- \rightarrow W^+W^-g\bar{b}\bar{b}$. Top: Average over trajectories in phase-space with increasingly soft gluon, bottom: Average over trajectories with increasingly collinear $q\bar{q}$ -pair.

significantly enlarged. For those two center-of-mass energies, we expect the pseudo-dipoles to yield a more physical interpretation of the subtraction term and thus a reduced variance during the integration. This is confirmed in Fig.5, which shows the evolution of the Monte-Carlo error during the integration. In the case of pseudo-dipole subtraction at or above threshold, the uncertainty is indeed substantially lower than for standard CS-dipoles. Below

$\sigma[\text{fb}]$	$\sqrt{s} = 3m_W$		$\sqrt{s} = 2m_t$		$\sqrt{s} = 4m_t$	
	CS	ID	CS	ID	CS	ID
RS	-0.00772(6)	-0.00140(5)	-0.52(3)	-2.85(1)	-9.5(4)	-5.3(1)
BVI	0.16143(13)	0.15506(13)	148.07(9)	150.55(9)	230.0(2)	226.0(2)
Σ	0.15371(14)	0.15366(14)	147.55(9)	147.70(9)	220.5(4)	220.7(2)

Table 1. NLO cross sections for $e^+e^- \rightarrow W^+W^-b\bar{b}$ at $\mu_R = m_t$ and varying center-of-mass energy, computed using standard CS subtraction terms (CS) or pseudo-dipoles (ID). The subtracted real-emission contributions (RS) were calculated using 10^7 phase-space points. The Born, virtual corrections and integrated subtraction terms (BVI) were calculated using $3 \cdot 10^6$ phase-space-points.

threshold the performance of pseudo-dipole subtraction is similar to the standard technique.

Our validation is completed by a comparison of a few selected differential cross sections in the two subtraction schemes. Fig. 6 displays the invariant mass of the (anti-)top quark reconstructed at the level of the $W^+W^-b\bar{b}$ final state from the W -boson and a b -jet with a matching signed flavor tag. The deviation plot shows excellent statistical compatibility between the two simulations. It also displays clearly that the pseudo-dipole subtraction technique by construction generates smaller statistical uncertainties than the standard CS subtraction method.

5 Conclusions

We have presented a technique that allows to preserve the virtuality of intermediate propagators in the computation of subtracted real-emission corrections to processes involving resonances. We have validated this approach in a simple fixed-order calculation and outlined how it can be generalized to more complicated processes. Due to the close correspondence with standard Catani-Seymour dipole subtraction, a matching to parton showers can be carried out in the MC@NLO or POWHEG methods in the future, thus paving the way for a precision measurement of processes involving for example single-top and top-quark pair production.

A Construction of phase-space trajectories

In this appendix we describe a generic method to generate phase-space trajectories approaching the soft or collinear limits of the hard matrix element, as used in Sec. 4.1. The technique is based on a suitable scaling of the Lorentz invariants parametrizing the desired limit. The corresponding kinematical configuration is determined by combining the appropriate final-state momenta using the massive dipole kinematics of [12] and subsequently constructing a new real-emission configuration by applying the techniques in [22].

We use the notation and definitions of [11] for final-state splittings with final-state spectator

$$\tilde{z}_i = \frac{p_i p_k}{(p_i + p_j) p_k}, \quad y_{i,j,k} = \frac{p_i p_j}{p_i p_j + (p_i + p_j) p_k}. \quad (\text{A.1})$$

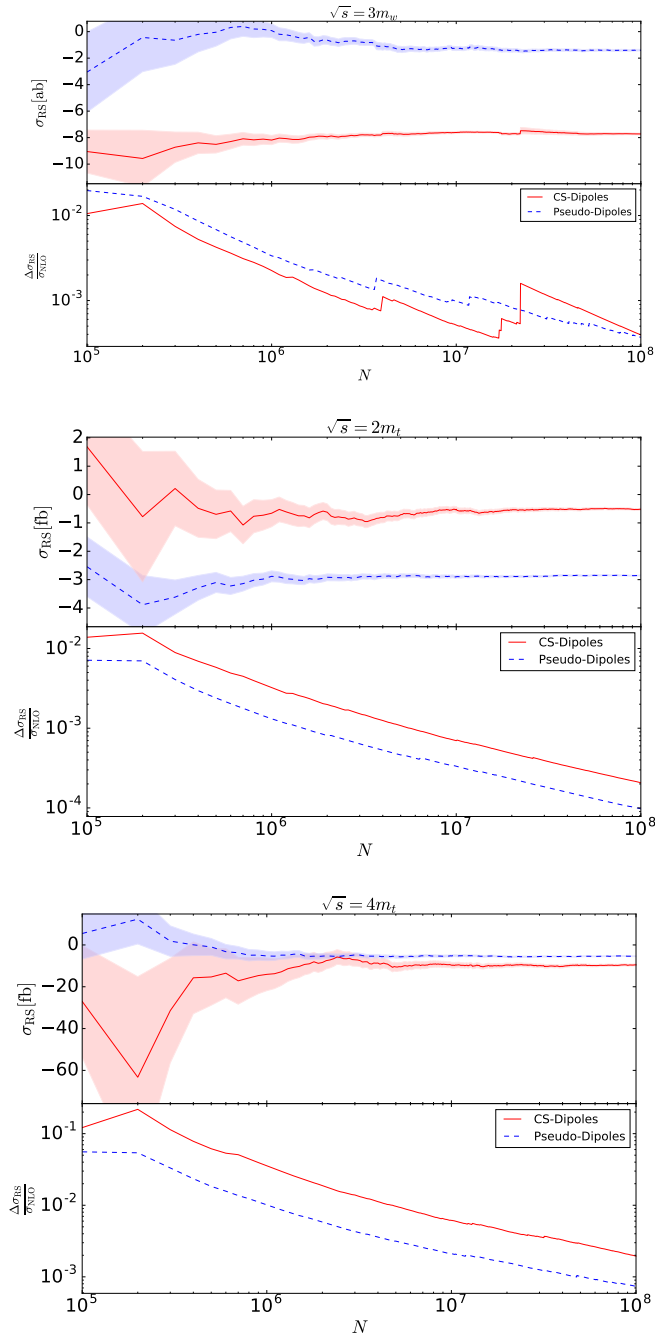


Figure 5. Evolution of the Monte-Carlo integration results for the subtracted real-emission contribution to the total cross section in $e^+e^- \rightarrow W^+W^-b\bar{b}$ at varying center-of-mass energy. From top to bottom: $\sqrt{s} = 3m_W$, $\sqrt{s} = 2m_t$ and $\sqrt{s} = 4m_t$. Red solid lines show results from standard CS-dipoles, while blue dashed lines correspond to pseudo-dipoles. The colored bands in the upper panels and the lines in the lower panels show the one σ statistical uncertainty of the Monte-Carlo integration.

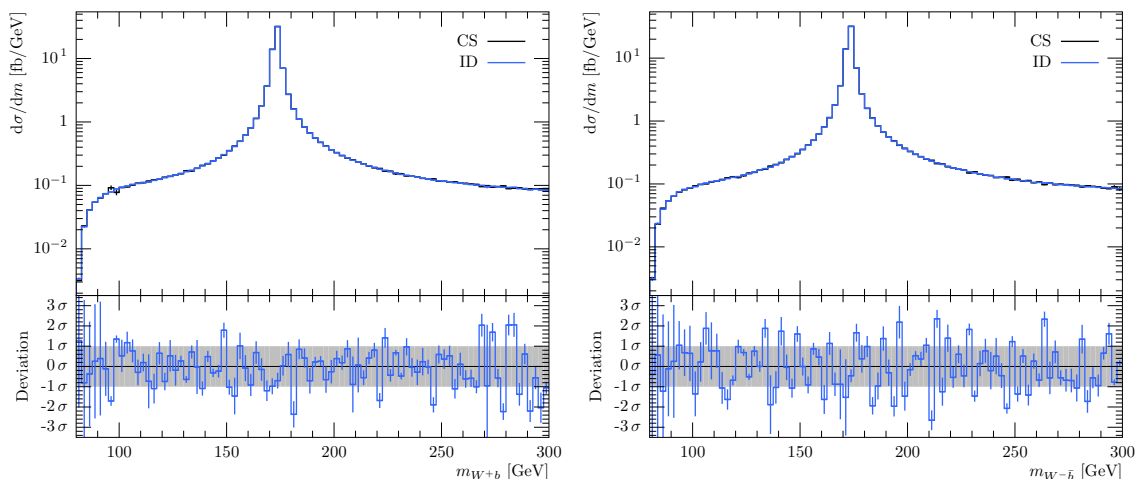


Figure 6. Invariant mass of the (anti-)top quark reconstructed at the level of the $W^+W^-b\bar{b}$ final state from the W -boson and a b -jet with a matching signed flavor tag.

	soft g		collinear $\bar{b}g$	
	CS $j \rightarrow \bar{b}, k \rightarrow b$	ID $j \rightarrow W^-, k \rightarrow \bar{b}$	CS $j \rightarrow \bar{b}, k \rightarrow b$	ID $j \rightarrow W^-, k \rightarrow \bar{b}$
y	λy	λy	λy	$y \frac{1 - \lambda \tilde{z}(1 - y)}{1 - \tilde{z}(1 - y)}$
\tilde{z}	$\lambda \tilde{z} \frac{1 - y}{1 - \lambda y}$	1	$\lambda \tilde{z}(1 - y)$	$\left[1 - y \frac{1 - \lambda \tilde{z}(1 - y)}{1 - \tilde{z}(1 - y)} \right]^{-1}$

Table 2. Scaling of Catani-Seymour parameters defined in Eq. (A.1) used to construct the phase-space trajectories in Sec. 4.1. The scaling parameter is denoted by λ , and the gluon is labeled as particle i .

Table 2 gives the assignment of the final-state momenta to the labels i, j and k for standard CS dipoles and pseudo-dipoles and shows how y and \tilde{z} are rescaled in order to construct the phase-space trajectories. The construction of momenta proceeds as follows: We first combine the three final-state momenta p_i, p_j and p_k into intermediate momenta \tilde{p}_k and $\tilde{p}_{ij} = q - \tilde{p}_k$, where $q = p_i + p_j + p_k$.

$$\tilde{p}_k^\mu = \left(p_k^\mu - \frac{q \cdot p_k}{q^2} q^\mu \right) \sqrt{\frac{\lambda(q^2, m_{ij}^2, m_k^2)}{\lambda(q^2, s_{ij}, m_k^2)}} + \frac{q^2 + m_k^2 - m_{ij}^2}{2q^2} q^\mu, \quad (\text{A.2})$$

where the Källén function is given by $\lambda(a, b, c) = (a - b - c)^2 - 4bc$. Using the scaled parameters y and \tilde{z} we compute the new mass of the pseudoparticle ij as $s_{ij} = y(q^2 - m_k^2) + (1 - y)(m_i^2 + m_j^2)$, and use Eq. A.2 with $\tilde{p}_k \leftrightarrow p_k$ and $m_{ij} \leftrightarrow s_{ij}$ to recalculate p_k

and p_{ij} . The new momentum p_i is then constructed as

$$p_i^\mu = \bar{z} \frac{\gamma(q^2, s_{ij}, m_k^2) p_{ij}^\mu - s_{ij} p_k^\mu}{\beta(q^2, s_{ij}, m_k^2)} + \frac{m_i^2 + k_\perp^2}{\bar{z}} \frac{p_k^\mu - m_k^2/\gamma(q^2, s_{ij}, m_k^2) p_{ij}^\mu}{\beta(q^2, s_{ij}, m_k^2)} + k_\perp^\mu, \quad (\text{A.3})$$

where $\beta(a, b, c) = \text{sgn}(a - b - c) \sqrt{\lambda(a, b, c)}$ and $2\gamma(a, b, c) = (a - b - c) + \beta(a, b, c)$. The parameters \bar{z} and $k_\perp^2 = -k_\perp^2$ of this decomposition are given by

$$\bar{z} = \frac{q^2 - s_{ij} - m_k^2}{\beta(q^2, s_{ij}, m_k^2)} \left[\tilde{z} - \frac{m_k^2}{\gamma(q^2, s_{ij}, m_k^2)} \frac{s_{ij} + m_i^2 - m_j^2}{q^2 - s_{ij} - m_k^2} \right], \quad (\text{A.4})$$

$$k_\perp^2 = \bar{z}(1 - \bar{z}) s_{ij} - (1 - \bar{z}) m_i^2 - \bar{z} m_j^2,$$

The transverse momentum is constructed using an azimuthal angle, ϕ_i

$$k_\perp^\mu = k_\perp \left(\cos \phi_i \frac{n_\perp^\mu}{|n_\perp|} + \sin \phi_i \frac{l_\perp^\mu}{|l_\perp|} \right), \quad (\text{A.5})$$

where

$$n_\perp^\mu = \epsilon^{0\mu}_{\nu\rho} \tilde{p}_{ij}^\nu \tilde{p}_k^\rho, \quad l_\perp^\mu = \epsilon^{\mu}_{\nu\rho\sigma} \tilde{p}_{ij}^\nu \tilde{p}_k^\rho n_\perp^\sigma. \quad (\text{A.6})$$

In kinematical configurations where $\vec{p}_{ij} = \pm \vec{p}_k$, n_\perp defined as in the definition of Eq. (A.5) vanishes. It can then be computed as $n_\perp^\mu = \epsilon^{0i\mu}_{\nu} \tilde{p}_{ij}^\nu$, where i may be any index that yields a nonzero result.

References

- [1] K. Agashe et al., *Working Group Report: Top Quark*, in *Proceedings, 2013 Community Summer Study on the Future of U.S. Particle Physics: Snowmass on the Mississippi (CSS2013): Minneapolis, MN, USA, July 29-August 6, 2013*, 2013. [1311.2028](#).
- [2] G. Heinrich, A. Maier, R. Nisius, J. Schlenk and J. Winter, *NLO QCD corrections to $W^+W^-b\bar{b}$ production with leptonic decays in the light of top quark mass and asymmetry measurements*, *JHEP* **06** (2014) 158, [[1312.6659](#)].
- [3] S. Frixione and B. R. Webber, *Matching NLO QCD computations and parton shower simulations*, *JHEP* **06** (2002) 029, [[hep-ph/0204244](#)].
- [4] S. Frixione, P. Nason and G. Ridolfi, *A Positive-weight next-to-leading-order Monte Carlo for heavy flavour hadroproduction*, *JHEP* **09** (2007) 126, [[0707.3088](#)].
- [5] T. Ježo and P. Nason, *On the Treatment of Resonances in Next-to-Leading Order Calculations Matched to a Parton Shower*, *JHEP* **12** (2015) 065, [[1509.09071](#)].
- [6] T. Ježo, J. M. Lindert, P. Nason, C. Oleari and S. Pozzorini, *An NLO+PS generator for $t\bar{t}$ and Wt production and decay including non-resonant and interference effects*, *Eur. Phys. J.* **C76** (2016) 691, [[1607.04538](#)].
- [7] R. Frederix, S. Frixione, A. S. Papanastasiou, S. Prestel and P. Torrielli, *Off-shell single-top production at NLO matched to parton showers*, *JHEP* **06** (2016) 027, [[1603.01178](#)].
- [8] S. Ferrario Ravasio, T. Ježo, P. Nason and C. Oleari, *A theoretical study of top-mass measurements at the LHC using NLO+PS generators of increasing accuracy*, *Eur. Phys. J.* **C78** (2018) 458, [[1801.03944](#)].

- [9] T. Ježo, J. M. Lindert, N. Moretti and S. Pozzorini, *New NLOPS predictions for $t\bar{t} + b$ -jet production at the LHC*, *Eur. Phys. J.* **C78** (2018) 502, [[1802.00426](#)].
- [10] S. Frixione, Z. Kunszt and A. Signer, *Three jet cross-sections to next-to-leading order*, *Nucl. Phys.* **B467** (1996) 399–442, [[hep-ph/9512328](#)].
- [11] S. Catani and M. H. Seymour, *A General algorithm for calculating jet cross-sections in NLO QCD*, *Nucl. Phys.* **B485** (1997) 291–419, [[hep-ph/9605323](#)].
- [12] S. Catani, S. Dittmaier, M. H. Seymour and Z. Trocsanyi, *The Dipole formalism for next-to-leading order QCD calculations with massive partons*, *Nucl. Phys.* **B627** (2002) 189–265, [[hep-ph/0201036](#)].
- [13] K. Fujii et al., *Physics Case for the International Linear Collider*, [1506.05992](#).
- [14] A. Arbey et al., *Physics at the e^+e^- Linear Collider*, *Eur. Phys. J.* **C75** (2015) 371, [[1504.01726](#)].
- [15] ATLAS collaboration, M. Aaboud et al., *Probing the quantum interference between singly and doubly resonant top-quark production in pp collisions at $\sqrt{s} = 13$ TeV with the ATLAS detector*, *Submitted to: Phys. Rev. Lett.* (2018) , [[1806.04667](#)].
- [16] T. Gleisberg and F. Krauss, *Automating dipole subtraction for QCD NLO calculations*, *Eur. Phys. J.* **C53** (2008) 501–523, [[0709.2881](#)].
- [17] S. Catani, Y. L. Dokshitzer, M. Olsson, G. Turnock and B. R. Webber, *New clustering algorithm for multijet cross sections in e^+e^- annihilation*, *Phys. Lett.* **B269** (1991) 432–438.
- [18] T. Gleisberg, S. Höche, F. Krauss, A. Schälicke, S. Schumann and J. Winter, *Sherpa 1.0, a proof-of-concept version*, *JHEP* **02** (2004) 056, [[hep-ph/0311263](#)].
- [19] T. Gleisberg, S. Höche, F. Krauss, M. Schönherr, S. Schumann, F. Siegert et al., *Event generation with Sherpa 1.1*, *JHEP* **02** (2009) 007, [[0811.4622](#)].
- [20] F. Krauss, R. Kuhn and G. Soff, *AMEGIC++ 1.0: A Matrix Element Generator In C++*, *JHEP* **02** (2002) 044, [[hep-ph/0109036](#)].
- [21] S. Jones and S. Kuttimalai, *Parton Shower and NLO-Matching uncertainties in Higgs Boson Pair Production*, *JHEP* **02** (2018) 176, [[1711.03319](#)].
- [22] S. Höche, S. Schumann and F. Siegert, *Hard photon production and matrix-element parton-shower merging*, *Phys. Rev.* **D81** (2010) 034026, [[0912.3501](#)].